Rapid Detection of Camouflaged Artificial Target Based on Polarization Imaging and Deep Learning

Ying Shen, Wenfu Lin, Zhifeng Wang, Jie Li, Xinquan Sun, Xianyu Wu, Shu Wang, and Feng Huang

***Abstract*—Polarization imaging has the advantage of detecting artificial targets based on their intrinsic characteristics. However, with the development of camouflage materials and camouflage shielding performance, the anti-optical detection technology for camouflaged targets continues to improve. In this paper, we combine the advantages of polarization imaging and deep learning to achieve rapid detection of artificial targets camouflaged in natural scenes. Firstly, we propose a Stokes-vector-based parameter image to show the polarization specificity of the camouflaged artificial targets. Then, a detection method is proposed, which uses an Otsu segmentation algorithm and morphological operations to extract polarization signatures of the target from the proposed parameter image, and utilizes the extracted polarization signatures to highlight the camouflaged artificial targets. Finally, we improve a self-supervised deep learning network to enhance the low-light images, extending the application of our method into low illumination environment target detection. Experimental results demonstrate that our method can effectively detect the camouflaged artificial targets with a detection rate better than 80%, which has potential application value in the fields of military target detection, security monitoring, and remote sensing.**

***Index Terms*—Camouflaged artificial target, deep learning, image processing, polarization imaging, target detection.**

I. Introduction

POLARIZATION, as one of the basic physical properties of light field besides amplitude, phase and frequency, has attracted increasing attention in recent years [1]. Polarization imaging technology has been applied in numerous fields, including remote sensing [2], medical diagnoses [3], defogging [4], underwater imaging [5], facial recognition [6], and target detection [7]. For the field of target detection, previous studies have shown that polarization imaging technology can improve the contrast between the artificial target and the natural background [8]–[12], and suppress cluttered signals from nature background [13], due to the material properties and surface roughness of artificial targets are different from those of natural backgrounds [14].

Compared with active polarization imaging [15], passive polarization imaging does not require a laser source and can capture the polarized solar radiation reflected by the target surface, thus having the advantage of imperceptibly detection of camouflaged artificial targets. Passive polarization imaging in the infrared wavelength can improve the accuracy of detecting artificial targets [16]. However, the spatial resolution of current infrared polarization imagery is insufficient to display the surface texture information on the artificial target [17]. Therefore, we consider passive polarization imaging in the visible wavelength to detect artificial targets camouflaged in nature scenes and obtain their surface texture information meanwhile.

During the last few decades, several kinds of polarimeters have been designed for passive polarization imaging, including the division-of-time, division-of-aperture and division-of-amplitude polarimeters [18]. Recently, due to the advancement in nanofabrication, the division-of-focal-plane (DoFP) polarimeter, which has a compact structure with micro-polarizers and micro-filters formed on chip, has aroused more interest [19], [20]. In this paper, we use a polarization camera (DoFP sensor) to realize the rapid detection of intensity, color and polarization signatures of the camouflaged artificial targets.

However, the on-chip structure of optical information multiplexing, such as micro-polarizers and micro-filters, reducing the luminous flux entering the DoFP sensor. As a result, although the polarization signatures of the camouflaged artificial targets can be detected in limited illumination conditions, the intensity information and color information about the natural scene are basically invisible. By increasing the exposure time, the imaging quality in limited illumination conditions can be improved, but the imaging frame rate will be reduced.

Deep learning has been proven to enhance low-light images. Chen *et al*. [21] developed a pipeline for processing low-light images, based on end-to-end training of a fully convolutional network. However, training this network requires a large number of paired training samples. Zhang *et al*. [22] proposed a self-supervised deep learning network to enhance low-light images. The training of this network only needs a small amount of low-light images and does not require paired training samples. Therefore, we improve this self-supervised deep learning network and train it to enhance the low-light images taken by our polarization camera. In this way, we can recognize the information of the natural scene while detecting the camouflaged artificial targets under a low illumination environment.

Manuscript received July 5, 2021; revised August 1, 2021; accepted August 6, 2021. Date of publication August 10, 2021; date of current version August 30, 2021. This work was supported in part by the National Natural Science Foundation of China under Grant 62005049, in part by the Natural Science Foundation of Fujian Province under Grant 2020J01451, in part by Education and Scientific Research Foundation for Young Teachers in Fujian Province under Grants JAT190003 and JAT190005, and in part by Fuzhou University Research Project under Grants GXRC-19052 and GXRC-18066. *(Ying Shen, Wenfu Lin, and Zhifeng Wang contributed equally to this work.) (Corresponding author: Shu Wang.)*

The authors are with the College of Mechanical Engineering and Automation, Fuzhou University, Fuzhou 350108, China (e-mail: yshen@fzu.edu.cn; bdlinwenfu@163.com; 15880277679@139.com; 2320420277@qq.com; 1173564986@qq.com; xwu@fzu.edu.cn; shu@fzu.edu.cn; huangf@fzu.edu.cn).

Digital Object Identifier 10.1109/JPHOT.2021.3103866

This work is licensed under a Creative Commons Attribution 4.0 License. For more information, see https://creativecommons.org/licenses/by/4.0/

This paper aims to use passive polarization imaging technology to detect artificial targets camouflaged in natural scenes, and to develop image processing algorithm to enhance the detection of artificial targets. Our detection method focuses on extracting polarization signatures of the target from the proposed parameter image and highlighting the camouflaged artificial targets in the polarization intensity image. In addition, we use the deep learning network to enable our detection method to detect artificial targets camouflaged under a low illumination condition. Our ultimate goal is to rapidly detect the camouflaged artificial targets under normal and low illumination conditions, which will bring polarization imaging and deep learning fully integrated into the realm of practicality for camouflage target detection.

II. Theory and Method

A. The Stokes Vector and Polarization Parameters

For passive polarization imaging in the visible wavelength, the solar radiation reflected by the smooth surfaces of the camouflaged artificial target becomes partially polarized, which can be described by a Stokes vector, $\mathbf{S} = (S_0, S_1, S_2, S_3)^T$. It is a column vector with four parameters. Among them, S_0 is the total light intensity; S_1 is the linearly polarized light component between horizontal and vertical directions; S_2 is the linearly polarized light component between 45° and 135° directions; and S_3 is the circularly polarized light component, which has been ignored by our polarization camera. Hence, the Stokes vector can be simplified and written as:

$$\mathbf{S}=\begin{bmatrix} S_0(x,y) \\ S_1(x,y) \\ S_2(x,y) \end{bmatrix} = \begin{bmatrix} I_0(x,y)+I_{90}(x,y) \\ I_0(x,y)-I_{90}(x,y) \\ I_{45}(x,y)-I_{135}(x,y) \end{bmatrix} \tag{1}$$

Where $I_0(x, y)$, $I_{45}(x, y)$, $I_{90}(x, y)$, and $I_{135}(x, y)$ are four intensity images with micro-polarizers oriented at 0°, 45°, 90°, and 135°, respectively. Through (1), it is obvious that after measuring the light intensity of the four polarization directions, the first three parameters of the Stokes vector can be calculated. Using these Stokes vector parameters, additional metrics can be calculated.

In previous studies [23], [24], the degree of linear polarization (DoLP) and angle of polarization (AoP) were two critical metrics that extensively used in target detection tasks. These two metrics can be calculated from the first three parameters of the Stokes vector using the following equations:

$$I_{\mathrm{DoLP}}(x,y) = \frac{\sqrt{S_1^2(x,y)+S_2^2(x,y)}}{S_0^2(x,y)} \tag{2}$$

$$I_{\mathrm{AoP}}(x,y) = \frac{1}{2}\arctan\left[\frac{S_2(x,y)}{S_1(x,y)}\right] \tag{3}$$

Differ from previous methods, which used color mapping codes to directly map S_0, DoLP, and AoP images into HSI color space to enhance man-made objects [25] [26], or used fusion algorithm of wavelet transform to fuse polarization images and intensity image to enhance target detection [27]. Our detection method has an additional step of extracting polarization signatures of the target from the polarization parameter image.

By analyzing DoLP and AoP images, we found that AoP image contains lots of noise and thereby is not suitable for extracting the target polarization signatures. The DoLP image also contains some noise because it is normalized by the S_0 parameter. Therefore, to facilitate the extraction of polarization signatures of the target, we modify the DoLP parameter.

According to (2), the completely polarized light component of the total light intensity is I_{P}, which is expressed as:

$$I_{\mathrm{P}}(x,y) = \sqrt{S_1^2(x,y)+S_2^2(x,y)} \tag{4}$$

In our experiments, we found that the I_{P} parameter image contains most of the polarization signatures of the camouflaged artificial targets, and S_1 parameter usually contains more target polarization signatures than S_2 parameter. Therefore, we added S_1 parameter to the second squared term of the I_{P} parameter to obtain more target polarization signatures. The proposed Stokes-vector-based I_{S} parameter is defined as:

$$I_{\mathrm{S}}(x,y) = \sqrt{S_1^2(x,y)+\left[S_2(x,y)+S_1(x,y)\right]^2} \tag{5}$$

The I_{S} parameter image outperforms DoLP parameter image in terms of the target/background contrast and contains less noise. Its high signal-to-noise ratio (SNR) allows us to accurately extract the polarization signatures of the camouflaged artificial targets.

B. The Camouflaged Artificial Target Detection Method

In order to effectively detect the artificial targets camouflaged in natural scenes under normal and low illumination conditions, we propose a detection method that combines polarization imaging and deep learning. First, a DoFP polarization camera is used to image the camouflaged artificial targets. The targets are initially enhanced by the polarization imaging technology. Second, image processing algorithm is developed to further enhance the camouflaged artificial targets in the S_0 Stokes image (also known as polarization intensity image). Moreover, a deep learning network is trained to enhance the low-light S_0 Stokes images. A flow chart of our method is shown in Fig. 1, which mainly includes the following four steps:

1) Original polarization image preprocessing: The original polarization image obtained by the DoFP polarization camera is split into four intensity images with different polarization directions; then the Stokes images and the proposed I_{S} parameter image can be calculated.
2) Polarization signature extraction: The Otsu algorithm is applied to I_{S} parameter image to extract polarization signatures of the target, and morphological operations are used to make our extraction results more accurate.
3) Low-light image enhancement: The deep learning network is trained to enhance low-light S_0 Stokes image, so as to detect artificial targets camouflaged under a low illumination environment.

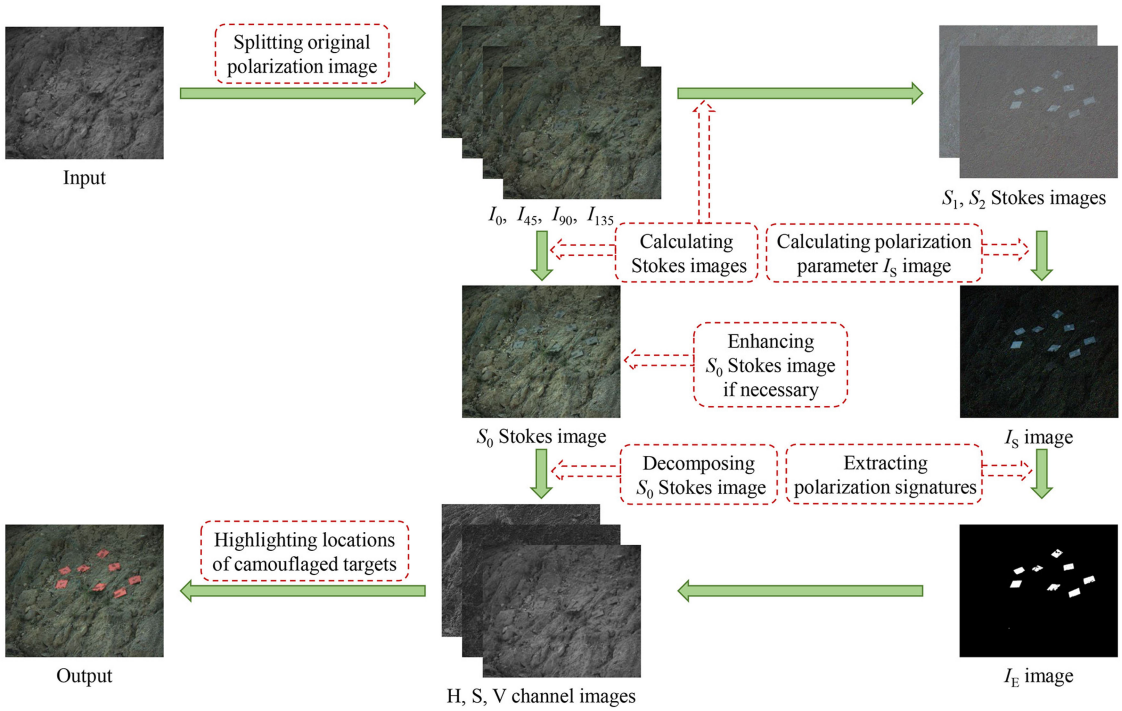

Fig. 1. The overall flowchart of our camouflaged artificial target detection method.

4) Highlighting target location: The extracted polarization signatures are used to highlight the locations of the camouflaged artificial targets in the polarization intensity image.

C. Pre-Processing Original Polarization Image

An original polarization image taken by our polarization camera is a mosaic grayscale image with a resolution of 2448×2048, in which each 2×2 super-pixel contains four directional polarization information (0°, 45°, 90°, and 135°) and one spectrum information (460nm, 530nm, or 625nm). The first step of our method is pre-processing the original polarization image. The raw image data are split into four polarized intensity images $I_0(x, y)$, $I_{45}(x, y)$, $I_{90}(x, y)$, and $I_{135}(x, y)$ by the Newton's polynomial interpolation algorithm [28], and the Bayer algorithm [29] is employed to convert each of them into a color image.

According to (1), the Stokes images can be calculated from these four polarized intensity images. Other polarization parameter images, including the I_S parameter image can also be calculated from the Stokes images. Fig. 2 shows the polarization parameter images in color. It can be seen that the I_S parameter image has higher contrast and higher SNR than the DoLP parameter image.

D. Extracting Polarization Signatures of the Camouflaged Artificial Target

The second step of our method is extracting polarization signatures of the camouflaged artificial targets from the I_S image. We implement this step based on Otsu's segmentation algorithm [30]. First, the three-channel color I_S image is converted into a single-channel grayscale image, then a threshold T is automatically selected by the Otsu segmentation algorithm to divide the pixels of the grayscale image into two categories: target and background. According to Otsu's theory, a pixel with a gray value greater than T will be marked white, otherwise it will be masked black. Therefore, a binary image of the I_S parameter image is obtained:

$$I_B(x, y) = \begin{cases} 1, I_S(x, y) > T \\ 0, I_S(x, y) \le T \end{cases} \tag{6}$$

Where $I_S(x, y)$ represents the gray value of a pixel with coordinates (x, y) in the grayscale I_S image. Fig. 3(a) shows the binary image of Fig. 2(f). Due to the high contrast and high

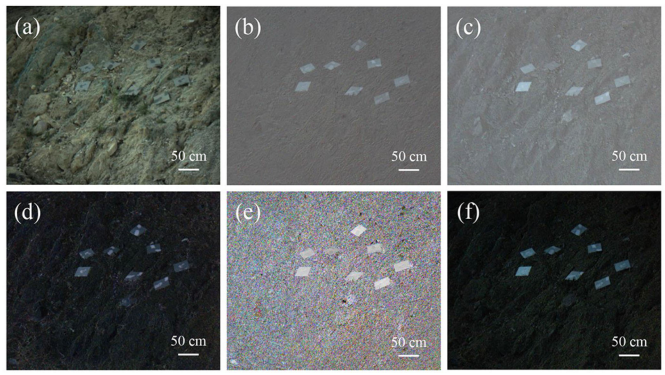

Fig. 2. Polarization parameter images in color. (a) S_0 Stokes image. (b) S_1 Stokes image. (c) S_2 Stokes image. (d) DoLP parameter image. (e) AoP parameter image. (f) The proposed polarization parameter I_S image.

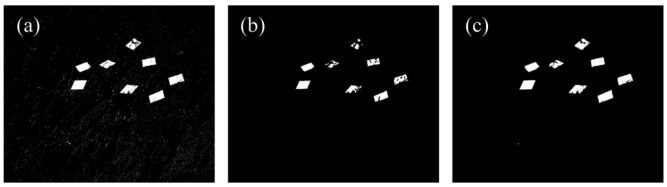

Fig. 3. The extracted polarization signatures of the camouflaged artificial targets. (a) A binary image of the I_{S} parameter image ($T = 0.22$). (b) The erosion map of (a) using a diamond shape structuring element with a size of 3×3. (c) The dilation map of (b) using the same structuring element.

SNR of the I_{S} parameter image, the polarization signatures of the camouflaged artificial targets can be extracted well.

However, some cluttered pixels of the natural background, such as small white dots in Fig. 3(a), are incorrectly classified as the polarization signatures of the target. In order to eliminate pixels that do not belong to the polarization signatures of the target, the morphological erosion operation is applied to Fig. 3(a). We have attempted several kinds of structuring elements for morphological erosion operation, among which a 3×3 diamond shape structuring element is the most suitable.

While removing these cluttered pixels, some pixels belonging to the target are also mistakenly removed, resulting in an incomplete extraction of the target polarization signatures, as shown in Fig. 3(b). In order to get a more complete target profile, the morphological dilation operation is applied to Fig. 3(b). The dilation map of Fig. 3(b) is obtained in Fig. 3(c). We call the dilation map as I_{E} image, because it is the extraction result of the target polarization signatures of the camouflaged artificial targets.

E. Enhancing the Low-Light S_0 Stokes Image

When detecting the artificial targets camouflaged under a low illumination environment, the third step of our method is to enhance the low-light S_0 Stokes images. Inspired by the powerful image enhancement capabilities of deep learning, we improved a self-supervised deep learning network and trained it to enhance the low-light S_0 Stokes images. Different from the network structure in Ref. [22], we improved its simple shallow convolutional neural network (CNN) into a deep CNN. We named this improved network Polar-Net, which is conducive to fully extract features of the low-light S_0 Stokes images and preserve details in the enhanced images.

As depicted in Fig. 4, the Polar-Net consists of the shallow feature extraction layer, the deep feature extraction layer, the up sampling layer, the down sampling layer, the feature refinement layer, the reconstruction layer and the decomposition layer. Firstly, one 9×9 convolutional layer is used to extract shallow information from the input image. In order to improve the memory ability of the shallow layers in the deep network, one 3×3 convolutional layer is used to preserve shallow features for subsequent deep convolution layers. Then the extracted shallow features were passed through deep features extraction layers which stacking from 27 convolutional layers followed by a ReLU activation function. In order to utilize the information of shallow layers and make the final image more clearly in texture details, we concatenated the first 3×3 convolutional layer with multiple deep convolutional layers to fuse the hierarchical information. In addition, the up-sampling and down-sampling operations were adopted to reduce the image noise. As explained previously, we use the concatenation to achieve the purpose of reusing the features and preserving more details. However, different hierarchical information is coarse during the incorporation. In order to address this issue, we proposed two information refinement layers to learn more accuracy features. The image reconstruction was implemented by a 3×3 convolutional layer with 4 output channels. Finally, the reflectance and illumination maps can be generated by the sigmoid function. It should be noted that, the reflectance map is the enhanced S_0 Stokes image that we need. The loss function of the Polar-Net is shown below:

$$Z = \|S - R \circ I\|_1 + \lambda_1 \left\| \max_{c\in R,G,B} R^c - F\left(\max_{c\in R,G,B} S^c\right) \right\|_1 + \lambda_2 \|\Delta I \circ \exp\left(-\lambda_3 \Delta R\right)\|_1 + \lambda_4 \|\Delta R\|_1 \quad (7)$$

Where S, R, and I denote the source image, reflectance and illumination maps, respectively. The symbol $\circ$ represents element-wise product.$\|S - R \circ I\|_1$ represents the reconstruction loss,$\lambda_1 \| \max_{c\in R,G,B} R^c - F(\max_{c\in R,G,B} S^c)\|_1 + \lambda_4 \|\Delta R\|_1$ represents the loss of the reflectance image, $\lambda_2 \|\Delta I \circ \exp(-\lambda_3 \Delta R)\|_1$ represents the structure-aware smoothness loss. The values of the weight parameters$\lambda_1, \lambda_2, \lambda_3, \lambda_4$ are 0.1, 0.1, 10, and 0.01 in our experiments.

We used a standard public LOL dataset [22] to train our improved deep learning model. This dataset comprises 485 pairs of training images, and 15 test images. We only used 485 low-light images to complete the network training. Our model is trained by the ADAM optimizer with the initial learning rate set to 0.001. We set the train epochs as 600 and evaluate the test images every 20 epochs. The model was implemented by 1.14 tensorflow framework, and all experiments were completed on an Nvidia GTX 2080Ti GPU and Inter Core i7-9700K CPU.

F. Highlighting the Camouflaged Artificial Target

The last step of our method is highlighting the camouflaged artificial targets in the S_0 Stokes image, exploiting the extracted polarization signatures. We converted the S_0 Stokes image from RGB color space to HSV color space, and decomposed it into H (hue), S (saturation), and V (value) channel images. The I_{E} image is used to determine whether a pixel in the S_0 Stokes image belongs to the camouflaged artificial target or the natural background.

In the I_{E} image, if the gray value of a pixel is 1, it means that it belongs to the camouflaged artificial target. The gray value of the corresponding position in the H channel image is doubled, and the gray values of the corresponding positions in the S channel image and the V channel image remain unchanged. If the gray value of a pixel in the I_{E} image is 0, it means that it belongs to the natural background. The gray values of the corresponding positions in the H channel image, S channel image, and V channel image remain unchanged. Finally, the

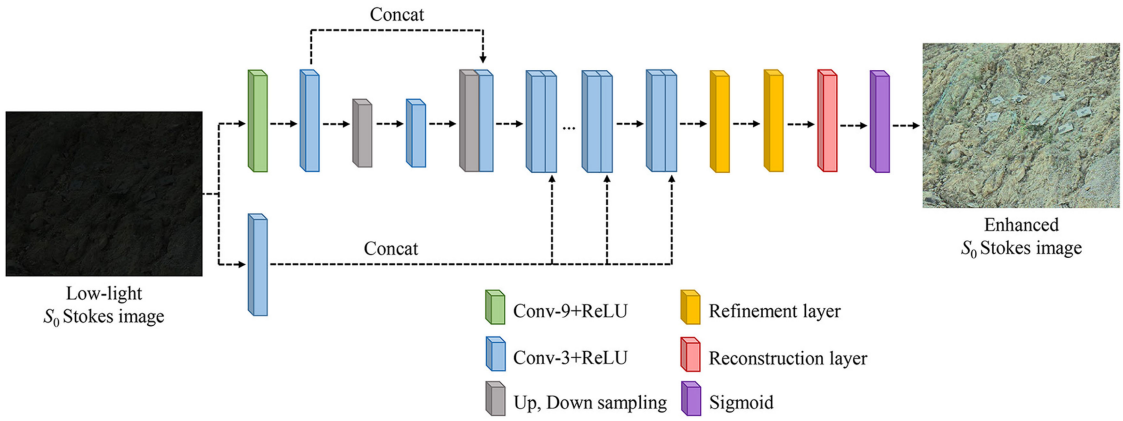

Fig. 4. The architecture diagram of the Polar-Net.

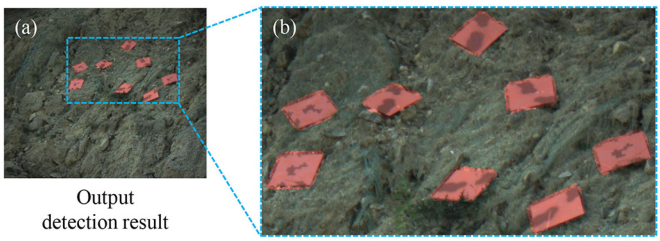

Fig. 5. The highlighted camouflaged artificial targets. (a) The output detection result obtained by our method. (b) An enlarged view of the region in (a) marked in blue.

Fig. 6. (a) FLIR color polarization camera. (b) The experimental environment of the grassland scene. (c) Camouflage plates. The blue box are two kinds of camouflage plates used in the grassland scene, and the red box are two kinds of camouflage plates used in the desert scene.

reconstructed image data are converted from HSV color space to RGB color space for display.

Through this method, the locations of the camouflaged artificial targets in the S_0 Stokes image are greatly highlighted, while the texture information of the target surface and the color information of the natural background are retained.

III. Experimental Results

A. Experimental Setup

We conducted field experiments to demonstrate the effectiveness of our detection method. The major equipment used in our experiments is a color polarization camera (FLIR, BFS-U3-51S5PC, 12-bit, resolution: 2248 × 2048, frame rate: 75 FPS), as shown in Fig. 6(a). Two lenses (MORITEX, ML-M5025UR) with focal lengths of 16mm and 35mm are employed to pair with the polarization camera. The experimental environment of the grassland scene is shown in Fig. 6(b), where the polarization camera is mounted on a tripod and connected to a laptop via a USB3.0 data cable. The targets used in our experiments are aluminum alloy plates painted with camouflage pigments, which are used to simulate the surface of the real camouflaged artificial target. The size of the camouflage plate is 30 cm×30 cm. Fig. 6(c) shows four kinds of camouflage plates with grassland camouflage pigment and desert camouflage pigment, and they are painted in two patterns. A laser rangefinder and a luminance photometer are used to measure the imaging distance and ambient light intensity.

TABLE I
Experimental Settings Under Normal Illumination Condition

Groups	Scene	Target number	Field of View (cm^2)	Imaging distance (m)	Light intensity (lux)
N1	Grassland	1	251 × 189	10	1800
N2	Grassland	1	550 × 413	10	1800
N3	Desert	8	550 × 413	10	6460
N4	Desert	8	880 × 660	35	7240

B. Detection Results Under Normal Illumination Condition

In order to verify our method can detect artificial targets camouflaged under normal illumination condition, we conducted four groups of experiments in grassland and desert scenes. The experiments were conducted at around 15:00. The weather was clear with a temperature of 25°C. Table I shows the experimental settings.

We first use the color polarization camera to image the camouflage plate in the grassland scene. As shown in Fig. 7(a1), the color of the camouflage plate in the S_0 Stokes image is similar to the grassland background, and it is difficult for us to distinguish the camouflage plate from the grassland background at a glance. With the polarization imaging technology, the camouflage plate is initially enhanced. We can distinguish the camouflage plate from the natural background in the I_S parameter image by their difference in polarization signatures.

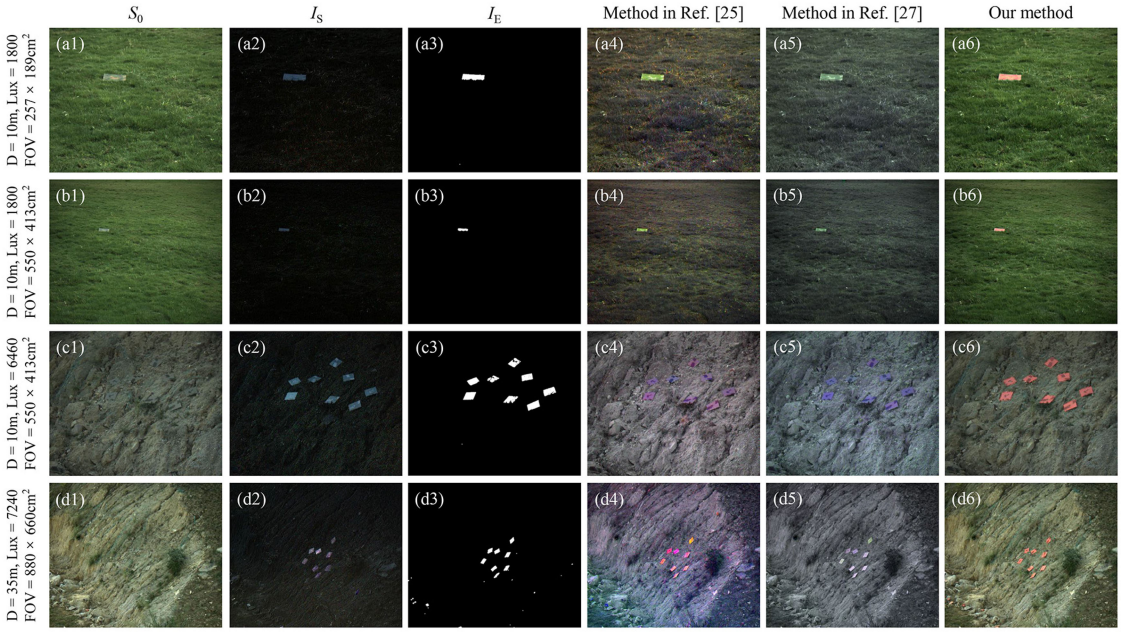

Fig. 7. Detection results under normal illumination condition. (a1–d1) S_0 Stokes images. (a2–d2) The proposed polarization parameter I_S images. (a3–d3) The I_E images which are the extraction results of the target polarization signatures. (a4–d4) The detection results of the method in Ref. [25]. (a5–d5) The detection results of the method in Ref. [27]. (a6–d6) The detection results of our method.

The I_S parameter image as shown in Fig. 7(a2) has enhanced the camouflage plate and suppressed the cluttered background. Subsequently, through image processing technique, the target polarization signatures can be extracted from the I_S parameter image. The extraction result is shown in Fig. 7(a3). It is utilized to further enhance the camouflage plate in the S_0 Stokes image. The detection result in Fig. 7(a6) indicates that our method can not only accurately detect the camouflaged artificial target from the natural background, but also improve the salience of the camouflaged artificial target in the polarization intensity image.

In order to further verify the universality of our method, we expanded the imaging field of view by reducing the focal length of the lens from 35mm to 16mm. Compared with Fig. 7(a1), the camouflage plate appears smaller in Fig. 7(b1) and is more difficult to be detected. From Fig. 7(b2), it is apparent that the camouflage plate has a polarization characteristic that is significantly different from the natural background. Therefore, the camouflage plate can be easily detected in the polarization parameter I_S image. The detection result in Fig. 7(b6) shows that our method can also distinguish small artificial target disguised in the natural background. In the desert scene, we increased the number of the camouflage plates to eight and randomly placed them on a barren land. As shown in Fig. 7(c1), the camouflage plates are well disguised in the desert background. They are almost invisible in the polarization intensity image. Through our detection method, multiple artificial targets camouflaged in the desert scene can be effectively detected at the same time [Fig. 7(c6)].

In order to simulate a more realistic desert scene, we conducted the fourth experiment in a complex barren land with many sandstones and weeds, as shown in Fig. 7(d1). Besides, the imaging distance was increased to 35 meters. From Fig. 7(d3), it can be seen that some cluttered pixels belonging to the natural background are incorrectly extracted as the polarization signatures of the target. However, these cluttered pixels have little effect on the final detection result. As can be seen in Fig. 7(d6), the appearance of a few cluttered pixels is permitted without affecting the target detection. Our method can still detect the artificial targets camouflaged in the complex desert scene.

TABLE II
EXPERIMENTAL SETTINGS UNDER LOW ILLUMINATION CONDITION

Groups	Scene	Target number	Field of View (cm^2)	Imaging distance (m)	Light intensity (lux)
L1	Grassland	1	251 × 189	10	8
L2	Grassland	1	550 × 413	10	8
L3	Desert	8	550 × 413	10	7
L4	Desert	8	880 × 660	35	5

C. Detection Results Under Low Illumination Condition

In order to verify our method can also detect artificial targets camouflaged under a low illumination condition, we performed another four groups of experiments in grassland and desert scenes. Fig. 8 shows four groups of images taken in the same scenes as shown in Fig. 7, but with different light intensity. The experimental settings are shown in Table II.

Different from Fig. 7, the images in Fig. 8 are taken in environments where the light intensity is lower than 10 lux. Under such a low illumination condition, the whole scene and the camouflage plates are basically invisible. Using the polarization imaging technology, the polarization signatures of the camouflage plates can be recognized in the I_S parameter image, as

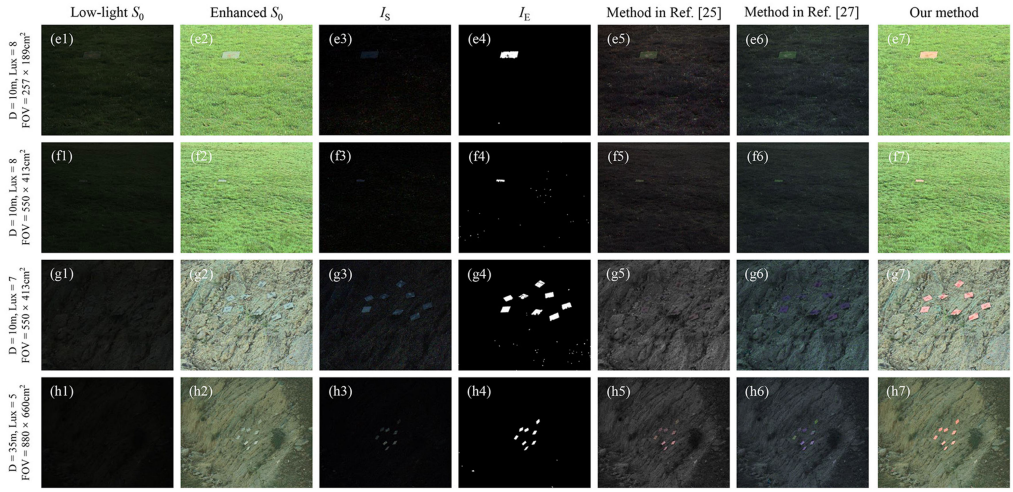

Fig. 8. Detection results under low illumination condition. (e1–h1) Low-light S_0 Stokes images. (e2–h2) Enhanced S_0 Stokes images. (e3–h3) The proposed polarization parameter I_S images. (e4–h4) The I_E images which are the extraction results of the target polarization signatures. (e5–h5) The detection results of the method in Ref. [25]. (e6–h6) The detection results of the method in Ref. [27]. (e7–h7) The detection results of our method.

shown in Fig. 8(e3 - h3). This implies that polarization imaging technology can reveal the camouflaged artificial targets under low illumination conditions, but the information of the natural background is almost invisible.

In order to recognize scene information when detecting artificial targets camouflaged under low illumination environments, we thereby trained the Polar-Net to enhance the low-light S_0 Stokes images. The enhancement results are shown in Fig. 8(e2–h2), which has clearly revealed the natural background. The I_E images in Fig. 8(e4–h4) are used to highlight the locations of the camouflage plates in the enhanced S_0 Stokes images. As shown in Fig. 8(e7–h7), our method can detect artificial targets camouflaged under low illumination conditions.

IV. Discussion

We compared our method with the color mapping code utilized to enhance man-made objects [25] and the fusion algorithm using wavelet transform [27]. With the color mapping code, polarization images (S_0, DoLP, and AoP) are directly mapped into HSI color space to synthesize a pseudo-color image to enhance the man-made objects. As for the fusion algorithm, it first maps S_0, DoLP, and AoP images into H, S, and I layers, and then uses the wavelet transform to reconstruct the wavelet coefficients of each layer. Finally, the man-made objects can be enhanced in the fusion image. The comparison results are shown in Fig. 7 and Fig. 8. They are shown in RGB color space for a fair comparison.

While the previous methods can be applied to enhance the camouflaged artificial targets, they also have some limitations. Firstly, they do not eliminate the polarization signatures of the cluttered background, which will reduce the accuracy of target detection. Secondly, the detection results obtained by the previous methods are synthetic pseudo-color images, which lose the real color information of the natural background. Thirdly, the salience of the camouflaged artificial targets in the detection results obtained by the previous methods needs to be further improved.

In order to prove that our method can highlight the camouflaged artificial targets to a greater extent, we calculated the color difference (D_C-value) between the camouflaged artificial target and the natural background according to (8).

$$D_C = \sqrt{(R_t - R_b)^2 + (G_t - G_b)^2 + (B_t - B_b)^2} \tag{8}$$

Where R_t, G_t, and B_t denote the average gray value of the pixels in the target region of the R, G, and B channels, respectively. R_b, G_b, and B_b denote the average gray value of the pixels in the background region of the R, G, and B channels, respectively. The calculation results are listed in Table III. It can be seen that the average D_C-value of our method is higher than that of the previous methods.

In order to prove that our method can accurately detect the camouflaged artificial targets, the detection results were processed by the threshold segmentation algorithm [33] and compared with the manually segmented ground truth images. We calculated the target detection rate (P_D) and false alarm rate (P_{FA}) according to (9) and (10).

$$P_D = \frac{N_t}{N_a} \tag{9}$$

$$P_{FA} = \frac{N_f}{N} \tag{10}$$

Where N_t is the number of target pixels correctly detected in our detection result; N_a is the actual number of target pixels in the ground truth image; N_f is the number of false alarm pixels in our detection result; and N is the number of pixels totally detected in our detection result. The calculation results are listed in Table IV.

As can be seen from Table IV, the average target detection rate of our method is 86.57%, which is higher than the previous methods. The average false alarm rate of our method is 8.19%, which is much lower than the previous methods. This demonstrates

TABLE III
THE D_C-VALUE OF DETECTION RESULTS FOR DIFFERENT METHODS

Methods	Normal illumination condition				Low illumination condition				Average
	N1	N2	N3	N4	L1	L2	L3	L4	
Method in Ref. [25]	0.539	0.599	0.218	**0.620**	0.206	0.267	0.096	0.277	0.353
Method in Ref. [27]	0.445	0.486	0.248	0.400	0.231	0.238	0.165	0.238	0.306
Our method	**0.810**	**0.849**	**0.567**	0.452	**0.582**	**0.562**	**0.485**	**0.585**	**0.608**

TABLE IV
TARGET DETECTION RATE AND FALSE ALARM RATE FOR DIFFERENT METHODS (%)

Metrics	Methods	Normal illumination condition				Low illumination condition				Average
		N1	N2	N3	N4	L1	L2	L3	L4	
P_D	Method in Ref. [25]	78.14	79.80	46.14	84.35	73.99	69.60	39.95	73.58	68.19
	Method in Ref. [27]	75.97	71.54	53.12	76.26	78.04	64.97	52.19	65.73	67.23
	Our method	**86.60**	**80.93**	**88.42**	**93.31**	**81.64**	**88.12**	**90.58**	**82.94**	**86.57**
P_{FA}	Method in Ref. [25]	54.03	60.66	95.91	96.97	77.90	82.79	96.81	82.33	80.93
	Method in Ref. [27]	52.69	51.03	96.25	71.49	72.76	73.07	97.42	80.87	74.44
	Our method	**3.96**	**0.93**	**1.76**	**27.48**	**4.65**	**2.37**	**4.61**	**19.79**	**8.19**

the ability of our method to accurately detect the camouflaged artificial targets with a low false alarm rate. However, it is worth noting that the false alarm rates of the N4 group and L4 group of our method are 27.48% and 19.79%, respectively, which are higher than other groups. It is because they were conducted in a more complex desert environment. The polarization signatures of some stones are similar to the camouflage plate, resulting in a higher false alarm rate. But they have little effect on the final detection results. In future research, we will continue to study how to reduce the false alarm rate of our detection method in a complex environment.

In this paper, the rapid refers to two parts. Firstly, in terms of imaging equipment, the DoFP polarization camera used in our experiments can achieve an imaging speed of 75 FPS, which is faster than the traditional polarization imaging mode of rotating the polarizer. Then, in terms of the running time of algorithm, the detection time of our algorithm is 0.82 seconds per frame, which is faster than the fusion algorithm in Ref. [27] (2.12 s/frame) and close to the color mapping code in Ref. [25] (0.75 s/frame). The deep learning algorithm takes 0.86 seconds to enhance a low-light polarization intensity image. We calculated the algorithm runtime on a computer configured with 16GB RAM and Inter Core i7-9700K CPU. However, our detection algorithm also has some limitations, for example, it cannot meet the requirements of real-time detection. In the future studies, we will continue to optimize the runtime of our detection algorithm through parallelization acceleration.

V. CONCLUSION

In this paper, we propose a method for detecting artificial targets camouflaged in natural scenes. Our detection method can accurately extract polarization signatures of the target from the polarization parameter image and highlight the camouflaged artificial targets in the polarization intensity image. In order to facilitate the extraction of polarization signatures, we propose a Stokes-vector-based parameter image, in which the contrast between the camouflaged artificial target and the natural background is improved. In order to extend the application of our method into low illumination environment target detection, we improve a self-supervised deep learning network to enhance the low-light polarization intensity images. In conclusion, our method makes it possible to rapidly detect artificial targets camouflaged in natural scenes under normal illumination and low illumination conditions.

However, there remains some limitations of our method. It is undeniable that the observational geometries have a great influence on the detection results. Under some imaging angles, our method cannot detect the camouflaged artificial targets. Future work will take into account the relationship between imaging angles and detection results. Besides, we will continue to develop algorithms that are more suitable for detecting small camouflaged artificial targets in a complex environment and optimize the algorithm runtime.

REFERENCES

[1] L. Yan, Y. Li, V. Chandrasekar, H. Mortimer, J. Peltoniemi, and Y. Lin, "General review of optical polarization remote sensing," *Int. J. Remote Sens.,* vol. 41, no. 13, pp. 4853–4864, 2020.

[2] W. Chen, L. Yan, and V. Chandrasekar, "Optical polarization remote sensing," *Int. J. Remote Sens.,* vol. 41, no. 13, pp. 4849–4852, 2020.

[3] R. Kodela and P. Vanagala, "Polarimetric parameters to categorize normal and malignant thyroid tissue," *IETE J. Res.,* vol. 63, no. 6, pp. 893–897, 2017.

[4] W. Zhang, J. Liang, F. Xing, Z. Man, X. Ge, and S. Fu, "Polarimetric imaging method for target enhancement in haze based on polarimetric retrieval," *J. Mod. Opt.,* vol. 66, no. 11, pp. 1235–1243, 2019.

[5] H. Hu, L. Zhao, X. Li, H. Wang, and T. Liu, "Underwater image recovery under the nonuniform optical field based on polarimetric imaging," *IEEE Photon. J.,* vol. 10, no. 1, Feb. 2018, Art. no. 6900309.

[6] A. J. Yuffa, K. P. Gurton, and G. Videen, "Three-dimensional facial recognition using passive long-wavelength infrared polarimetric imaging," *Appl. Opt.,* vol. 53, no. 36, pp. 8514–8521, 2014.

[7] R. Sun, X. Sun, F. Chen, H. Pan, and Q. Song, "An artificial target detection method combining a polarimetric feature extractor with deep convolutional neural networks," *Int. J. Remote Sens.,* vol. 41, no. 13, pp. 4995–5009, 2020.

[8] M. Wan, G. Gu, W. Qian, K. Ren, and Q. Chen, "Stokes-vector-based polarimetric imaging system for adaptive target/background contrast enhancement," *Appl. Opt.,* vol. 55, no. 21, pp. 5513–5519, 2016.

[9] F. Tang, L. Gui, J. Liu, K. Chen, L. Lang, and Y. Cheng, "Metal target detection method using passive millimeter-wave polarimetric imagery," *Opt. Exp.,* vol. 28, no. 9, pp. 13336–13351, 2020.

[10] J. Liang, W. Zhang, L. Ren, H. Ju, and E. Qu, "Polarimetric dehazing method for visibility improvement based on visible and infrared image fusion," *Appl. Opt.,* vol. 55, no. 29, pp. 8221–8226, 2016.

[11] M. Boffety, H. Hu, and F. Goudail, "Contrast optimization in broadband passive polarimetric imaging," *Opt. Lett.,* vol. 39, no. 23, pp. 6759–6762, 2014.

[12] F. Goudail and M. Boffety, "Optimal configuration of static polarization imagers for target detection: Erratum," *J. Opt. Soc. Amer. A,* vol. 33, no. 9, pp. 1812–1813, 2016.

[13] J. Liang, X. Wang, Y. Fang, J. Zhou, S. He, and W. Jin, "Water surface-clutter suppression method based on infrared polarization information," *Appl. Opt.,* vol. 57, no. 16, pp. 4649–4658, 2018.
[14] H. Zhan, D. G. Voelz, and M. Kupinski, "Parameter-based imaging from passive multispectral polarimetric measurements," *Opt. Exp.,* vol. 27, no. 20, pp. 28832–28843, 2019.
[15] N. Vannier *et al.*, "Comparison of different active polarimetric imaging modes for target detection in outdoor environment," *Appl. Opt.,* vol. 55, no. 11, pp. 2881–2891, 2016.
[16] H. Zhao, Z. Ji, Y. Zhang, X. Sun, P. Song, and Y. Li, "Mid-infrared imaging system based on polarizers for detecting marine targets covered in sun glint," *Opt. Exp.,* vol. 24, no. 15, pp. 16396–16409, 2016.
[17] X. Li and Q. Huang, "Target detection for infrared polarization image in the background of desert," in *Proc. IEEE Int. Conf. Commun. Softw. Netw.*, 2017, pp. 1147–1151.
[18] J. S. Tyo, D. L. Goldstein, D. B. Chenault, and J. A. Shaw, "Review of passive imaging polarimetry for remote sensing applications," *Appl. Opt.,* vol. 45, no. 22, pp. 5453–5469, 2006.
[19] T. York and V. Gruev, "Characterization of a visible spectrum division-of-focal-plane polarimeter," *Appl. Opt.,* vol. 51, no. 22, pp. 5392–5400, 2012.
[20] X. Tu *et al.*, "Division of focal plane red-green-blue full-Stokes imaging polarimeter," *Appl. Opt.,* vol. 59, no. 22, pp. G33–G40, 2020.
[21] C. Chen, Q. Chen, J. Xu, and V. Koltun, "Learning to see in the dark," in *Proc. IEEE Comput. Soc. Conf. Comput. Vis. Pattern Recognit.*, 2018, pp. 3291–3300.
[22] Y. Zhang, X. Di, B. Zhang, and C. Wang, "Self-supervised image enhancement network: Training with low light images only," 2020, *arXiv:2002.11300*.
[23] D. A. Lavigne, M. Breton, G. Fournier, M. Pichette, V. Rivet, and I. Kadar, "Development of performance metrics to characterize the degree of polarization of man-made objects using passive polarimetric images," in *Proc. SPIE-Int. Soc. Opt. Eng.,* 2009, pp. 73361A–73361A.
[24] X. Zeng, Y. Luo, X. Zhao, and W. Ye, "An end-to-end fully-convolutional neural network for division of focal plane sensors to reconstruct S0, DoLP, and AoP," *Opt. Exp.,* vol. 27, no. 6, pp. 8566–8577, 2019.
[25] J. S. Tyo, E. N. Pugh, and N. Engheta, "Colorimetric representations for use with polarization-difference imaging of objects in scattering media," *J. Opt. Soc. Amer. A,* vol. 15, no. 2, pp. 367–374, 1998.
[26] D. Lavigne *et al.*, "Target discrimination of man-made objects using passive polarimetric signatures acquired in the visible and infrared spectral bands," in *Proc. SPIE-Int. Soc. Opt. Eng.,* 2011, pp. 816007–816007.
[27] Q. C. Wang, J. C. Wang, D. P. Zhao, L. F. Ma, and Z. G. Li, "Recognition of camouflage targets with hyper-spectral polarization imaging system," in *Proc. SPIE-Int. Symp. Photoelectron. Detect. Imag.,* 2013, pp. 89101Q-89101Q.
[28] N. Li, Y. Zhao, Q. Pan, and S. G. Kong, "Demosaicking DoFP images using newton's polynomial interpolation and polarization difference model," *Opt. Exp.,* vol. 27, no. 2, pp. 1376–1391, 2019.
[29] B. Zhu, D. S. Wen, W. Gao, Z. X. Song, and H. Li, "Research and design of color restoration algorithm for demosaicing bayer pattern images," *Appl. Mech. Mater.,* vol. 130-134, pp. 745–751, 2012.
[30] N. Otsu, "A threshold selection method from gray-level histograms," *IEEE Trans. Syst. Man Cybern.,* vol. SMC-9, no. 1, pp. 62–66, Jan. 1979.